International Journal of Heat and Mass Transfer 52 (2009) 1701–1708

Contents lists available at ScienceDirect

International Journal of Heat and Mass Transfer

journal homepage: www.elsevier.com/locate/ijhmt

Instability phenomena in a two-phase microchannel thermosyphon

Patrick T. Garrity, James F. Klausner *, Renwei Mei

University of Florida, Mechanical and Aerospace Engineering, Gainesville, FL 32611, USA

ARTICLE INFO

Article history:
Received 15 April 2008
Received in revised form 2 October 2008
Available online 6 December 2008

Keywords:
Ledinegg
Instability
Two-phase
Thermosyphon
Microchannel

ABSTRACT

The behavior of a two-phase thermosyphon, consisting of a microchannel evaporator plate and a condenser, is investigated to gain insight into the system limiting instability. A microchannel plate has been fabricated with 56 square channels that have a 1×1 mm cross section and a length of 115 mm. Experiments have been conducted for various condenser heights with the heat flux as the control variable. A step increase in heat flux is used to quantify the response of the system, including variations in mass flow rate, temperature, and pressure drop. Results show that small fluctuations about the steady state give rise to the instability for situations with a uniform heat load. A predictive model based on the momentum equation is introduced to estimate the onset of instability, and the threshold heat flux is predicted to within ±10% uncertainty.

1. Introduction

Two-phase flow system instabilities and thermo-hydraulic oscillations have long been of interest in the energy field since many steam generators operate in the natural circulation mode. The two-phase instability phenomenon was first reported by Ledinegg [1] when investigating two-phase flow in steam generators. The onset of instabilities can be found in other applications involving passively driven two-phase flow systems, such as thermosyphons for electronic cooling and the present application, fuel cell thermal management. A number of reviews have considered two-phase flow instability phenomena, including those of Boure et al. [2], Ishi [3], Bergles [4], Yadigaroglu et al. [5], Fukuda and Kobori [6], and Kakac and Bon [7]. Instabilities in forced convection two-phase flow systems can be categorized as static or dynamic. Static instabilities include Ledinegg, boiling crisis, flow pattern transitions, bumping, chugging, or geysering. Dynamic instabilities include density wave, acoustic, pressure drop, and thermal oscillations, in addition to multi-channel and BWR.

Boure et al. [2] provide a more detailed description on the various instabilities reported. Numerous studies have been conducted to observe the mechanisms responsible for the onset of instability under natural circulation conditions [8–13]. For natural circulation systems, Yang et al. [11], Prasad et al. [12], and Jiang et al. [13], describe instabilities unique to passively driven flow, which are initially triggered by the static Ledinegg instability prior to transitioning to a pressure drop [14] and natural circulation instability. Instability phenomena associated with two-phase flow through narrow spaces is described by Tadrist [15]. It is shown that instability can arise in small channels due to the onset of local dryout.

An experimental investigation that focuses on understanding and predicting the onset of instability within a two-phase microchannel thermosyphon facility is presented. Since it is a passive flow system, the emphasis is on the static Ledinegg instability. The experimental facility incorporates a fixed geometry with variable condenser height. The applied heat flux is the control variable, while the system flow rate is a dependent variable. Under these operating conditions, small scale flow perturbations that occur under quasi-steady state conditions are measured and used to predict the onset of instability. To validate these predictions, both the pressure drop as well as the limiting heat flux are compared against those determined experimentally. The limiting heat flux is satisfactorily predicted to within ± 10% uncertainty. The uncertainty in the model prediction arises from uncertainties in the frictional pressure gradient and vapor volume fraction models.

2. Experimental considerations

2.1. Facility

The experimental two-phase thermosyphon is shown in Fig. 1. The cooling plate assembly includes 56 microchannels, 115 mm in length, and having a 1×1 mm cross section. A Minco foil heater is positioned on the backside of the microchannel plate and provides a maximum uniform heat flux of 70 kW/m^2. A lexan cover plate is stacked on top of the microchannels and allows for flow visualization. During operation, HFE-7100 circulates between the cooling plate and condenser. The condenser may be raised or

* Corresponding author. Tel.: +1 352 392 3506; fax: +1 352 392 1071.
E-mail address: klaus@ufl.edu (J.F. Klausner).

0017-9310/$ - see front matter © 2008 Elsevier Ltd. All rights reserved.
doi:10.1016/j.ijheatmasstransfer.2008.10.005

Nomenclature

C_0	distribution parameter
C_p	constant pressure specific heat (J/kg K)
d	hydraulic diameter (m)
f	friction factor
G	mass velocity (kg/m^2 s)
H	condenser height (m)
g	gravitational constant (m/s^2)
h_{fg}	latent heat of vaporization (J/kg)
$\dot{m}$	mass flow rate (kg/s) or (g/s)
P	pressure (Pa) or (kPa)
$\dot{q}$	heat rate (W)
Re	reynolds number
T	temperature (°C)
V_{vj}	drift velocity (m/s)
X	vapor quality
u_v	superficial vapor velocity (m/s)
z	axial location (m)

Greek symbols

α	vapor volume fraction
v	kinematic viscosity (m^2/s)
θ	inclination angle (radians)
ρ	density (kg/m^3)
σ	surface tension (N/m)
ΔP_s	total system pressure drop (Pa)

Subscripts

2φ	two-phase mixture
a	accelerational component
e	exit
f	frictional component
g	gravitational component
i	inlet
l	liquid
m	mixture
v	vapor
z	z-location

lowered in order to change the gravitational head driving the flow through the facility. A more detailed description of the experimental facility is reported in [16].

2.2. Experimental protocol

The condenser is positioned above the evaporator plate at one of four different heights considered for this investigation, 1.33, 1.15, 0.97, and 0.79 m. HFE-7100 is first added to the system until the liquid height is just below the condenser coils. All pressure lines are then carefully inspected for air bubbles, followed by the purging of all pressure transducers. A heat load is applied to the evaporator plate to generate vigorous boiling. The pressure release valve, located at the top of the condenser, is opened to purge all non-condensable gas from the system and improve condenser performance. The heat load is then reduced to zero so that the flow through the facility ceases. The heat flux is raised in small increments. At each increment the flow rate and temperatures are allowed to reach a quasi-steady state. Measurements of pressure, flow rate, and temperature are made at each heat flux interval. The heat flux is raised until large scale flow oscillations and flow reversal are easily visible; it is this flow condition that is deemed as unstable. The condenser height is then repositioned and the experiment is repeated.

2.3. System subcooling and manifold pressure drop

The temperature of the working fluid leaving the condenser is subcooled to some degree. At relatively low heat flux where no boiling takes place, the fluid is significantly below the saturation temperature, ΔT_{sub} = 10–40 °C. With a heat load of approximately 5 kW/m^2, vapor bubbles are observed in the riser. The vapor enters

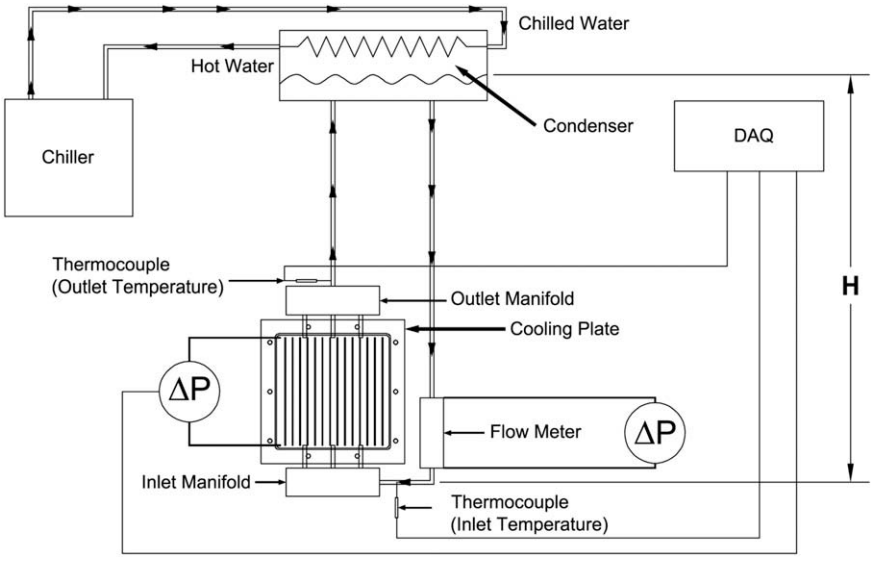

Fig. 1. Experimental two-phase thermosyphon facility.

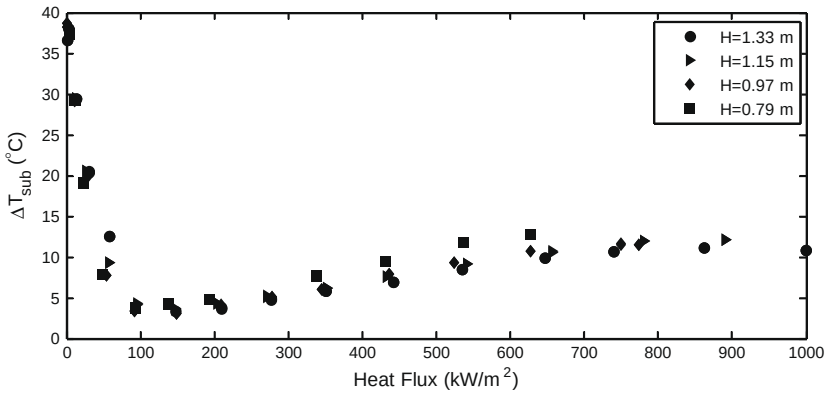

Fig. 2. Variation of inlet subcooling with heat flux.

the condenser and back into the bulk liquid. Fig. 2 shows the degree of subcooling measured for each heat flux and condenser height considered. At higher heat flux more vapor comes in contact with the coils, and as the heat flux is increased, the degree of subcooling becomes larger. Since the degree of subcooling affects vapor generation, the onset of instability depends on the inlet temperature to the evaporator. Measurements of subcooling have been made at each heat flux interval, and are shown in Fig. 2.

The pressure drops across the evaporator plate manifolds contribute significantly to the total pressure drop in the riser portion of the thermosyphon. Since the manifold design is unique to this experiment, direct measurements of pressure drop have been made at each heat load interval and condenser height and are shown in Fig. 3. The pressure drops through the inlet manifold correlates with liquid velocity and that for the exit manifold correlates with vapor superficial velocity and are shown in Fig. 3. The vapor superficial velocity is,

$$u_v = \frac{Gx(z)}{\rho_v}, \tag{1}$$

where G is the mass flux, $x(z)$ is the vapor quality at an axial location along the evaporator plate and ρ_v is the vapor density. The vapor quality is determined from an energy balance,

$$x(z) = \frac{\dot{q}_z - \dot{m}C_p[T(z) - T_i]}{\dot{m}h_{fg}}, \tag{2}$$

Here, $\dot{q}_z$ is the net rate of heat flow into the system at a specific z location, $T(z)$ is the bulk fluid temperature at axial location z, T_i is the measured evaporator plate inlet bulk temperature. The vapor quality is determined at the exit of the evaporator plate using the measured exit temperature of the bulk fluid, T_e in order to compute the exit manifold superficial velocity. As shown the inlet manifold pressure drop is larger than that at the outlet manifold where two-phase flow is present. For simplification, the pressure taps for the inlet manifold were located so that the pressure drop across the flow meter could be included in the measurement. It should also be noted that the pressure loss across the inlet manifold shown in Fig. 3 includes a small amount of tubing and a 90 degree bend.

3. Flow modeling

In order to predict the flow rate circulating through the thermosyphon loop, the momentum equation is used to compute the pressure gradient. The two-phase pressure gradient is comprised of three components: that due to gravity, friction, and acceleration denoted by the respective subscripts g, f, and a in Eq. (3),

$$\left(\frac{dP}{dz}\right)_{2\phi} = \left(\frac{dP}{dz}\right)_g + \left(\frac{dP}{dz}\right)_f + \left(\frac{dP}{dz}\right)_a. \tag{3}$$

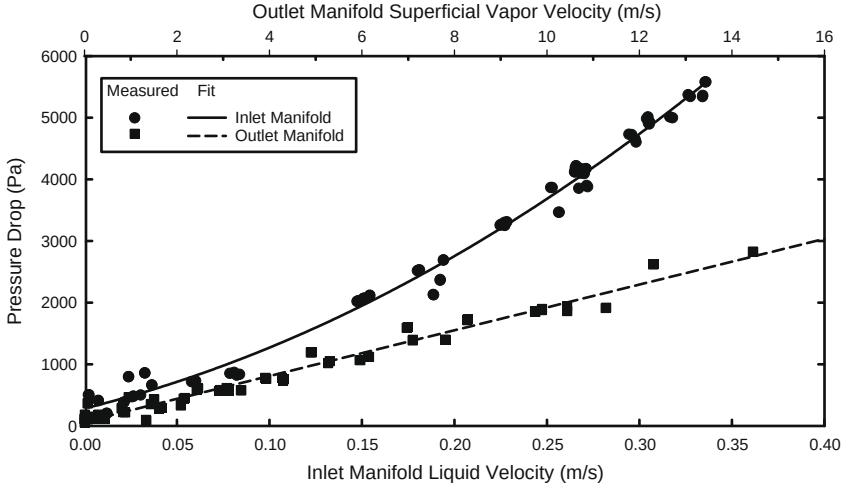

Fig. 3. Pressure drop across inlet and outlet manifolds.

In the case of a closed circulation loop, the difference in pressure between the discharge and return of the condenser is considered negligibly small. Therefore computing the pressure field throughout the thermosyphon loop allows determination of the mass flow rate, $\dot{m}$. The flow rate is computed as that which gives the same pressure at the inlet and outlet of the condenser. The gravitational pressure gradient component depends on the liquid–vapor mixture density and the gravity vector,

$$-\left(\frac{dP}{dz}\right)_g = \rho_m g \sin\theta, \tag{4}$$

where ρ_m is the mixture density, g is gravity, and θ is the inclination angle with respect to the horizontal. The mixture density is,

$$\rho_m = \alpha\rho_v + (1-\alpha)\rho_l. \tag{5}$$

The vapor volume fraction, α, is estimated using the Zuber-Findlay drift flux model [17] for slug flow,

$$\alpha = \left[C_0\left\{1+\left(\frac{1-x}{x}\right)\frac{\rho_v}{\rho_l}\right\}+\frac{\rho_v}{Gx}V_{vj}\right]^{-1}, \tag{6}$$

$$V_{vj} = 1.53\left(g\sigma\frac{(\rho_l-\rho_v)}{\rho_l^2}\right)^{1/4}. \tag{7}$$

Here $C_0 = 1.2$ is the distribution parameter. A momentum balance on a differential element is used to determine the accelerational pressure gradient component,

$$-\left(\frac{dP}{dz}\right)_a = G^2\frac{d}{dz}\left[\frac{(1-x)^2}{\rho_l(1-\alpha)}+\frac{x^2}{\rho_v\alpha}\right]. \tag{8}$$

As suggested by Garrity et al. [16], the frictional pressure gradient is computed using the Mueller-Steinhagen and Heck [18] correlation,

$$-\left(\frac{dP}{dz}\right)_f = F(1-x)^{1/3}+Bx^3, \tag{9}$$

$$F = A + 2(B-A)x, \tag{10}$$

$$A = f_l\frac{G^2}{2\rho_l d}, \tag{11}$$

$$B = f_v\frac{G^2}{2\rho_v d}. \tag{12}$$

Here d is the hydraulic diameter and the Darcy friction factors are computed as

$$f_l = \begin{cases} \frac{64}{Re_l}, & Re_l < 1187 \\ \frac{0.3164}{Re_l^{1/4}}, & Re_l > 1187 \end{cases} \tag{13}$$

$$f_v = \begin{cases} \frac{64}{Re_v}, & Re_v < 1187 \\ \frac{0.3164}{Re_v^{1/4}}, & Re_v > 1187 \end{cases} \tag{14}$$

$$Re_l = \frac{Gd}{\nu_l}, \tag{15}$$

$$Re_v = \frac{Gd}{\nu_v}. \tag{16}$$

In order to compute the local vapor quality, $x(z)$, from Eq. (2), the temperature field, $T(z)$ is computed using the Saha-Zuber [19] model for subcooled boiling. Using Eqs. (2)–(16) and the empirically determined pressure drop across the manifolds, the change in pressure from the condenser discharge to the inlet is computed. The mass flow rate is taken as that which yields no net change in total system pressure, ΔP_s. This is expressed as

$$\Delta P_s = \oint \left.\frac{dP}{dz}\right|_{2\phi} dz = 0 \tag{17}$$

4. Experimental results

The variation of the steady state mass flow rate of HFE-7100 circulating through the two-phase thermosyphon system with various applied heat fluxes is shown in Fig. 4 for different condenser elevations. At low heat loads the flow rate increases rapidly with increasing heat flux due to the increasing difference in pressure head between the riser and downcomer. This increase in pressure head results from the increasing vapor volume fraction. At slightly higher heat flux, the vapor quality becomes more significant and an increase in frictional pressure drop is observed. As the frictional pressure drop becomes more substantial, the flow rate begins to decrease. Although the mixture density in the riser is low, the high velocity and frictional dissipation results in a decreasing flow rate. The largest flow rate occurs when the condenser elevation above the microchannel evaporator plate is highest. This is because a larger difference in pressure head between the riser and downcomer is achieved when the condenser elevation is largest. The pressure drop variation across the microchannel plate with respect to mass flow rate is shown in Fig. 5. For $H = 0.97$ and 0.79 m, the predicted pressure drop decreases with increasing flow rate under relatively low heat flux. This is a result of operating at low vapor quality, where the frictional pressure drop approaches that of single phase flow. Also at low vapor quality, the vapor volume fraction increases significantly with small changes in quality, and the gravitational change in pressure drop is smaller at higher volume fraction. Thus a decrease in pressure drop is predicted. Given the complex nature of two-phase flow, the pressure drop prediction across the microchannel plate is considered to be in reasonable agreement with the measured data.

The reported uncertainty associated with the two-phase frictional pressure drop computed with the Mueller-Steinhagen and Heck [18] correlation is approximately ±41% while the uncertainty associated with the void fraction computed with the Zuber-Findlay [17] correlation is approximately ± 2.5%. In order to determine the uncertainty bounds of the mass flow rate predictions, the mass flow rate is computed using the upper and lower bounds of the frictional pressure drop and vapor volume fraction. Fig. 6 shows the upper and lower bounds of the predicted flow rates for $H = 1.33$ and 1.15 m. The measured flow rates are compared with those predicted bounds. Only two condenser elevations are presented for discussion purposes. As shown, the measured flow rates generally fall within the predicted bounds, thus providing further confirmation that the agreement between the measured flow rates and those predicted is reasonable.

The heat fluxes shown in Fig. 4 range from zero to a maximum value, at which point the system goes unstable. The system limiting heat flux for each condenser height is tabulated in Table 1. As observed, the limiting heat flux increases with increasing elevation of the condenser above the microchannel evaporator plate.

While the quasi-steady mass flow rate and pressure drop are very important variables for understanding the response of the system to step increases in heat flux, apparent random variations about the quasi-steady variables are equally important. It is the variation from the quasi-steady state that can send the two-phase thermosyphon into an unstable operating mode. Therefore, the stochastic variations in pressure drop and flow rate are examined. Figs. 7 and 8 show the probability density functions for both the pressure drop and flow rate immediately prior to encountering the flow instability for both $H = 1.33$ and 1.15. In each case the skewness is almost zero and the kurtosis is near to three, suggesting the distribution is close to normal. The percent fluctuation, defined here as the ratio of the standard deviation to the mean, is 11% for the pressure drop and 4.1% for the flow rate for $H = 1.33$ m. For $H = 1.15$ m., the percent fluctuation is 12% for the pressure drop and 6% for the flow rate. The percent fluctuations are not statisti-

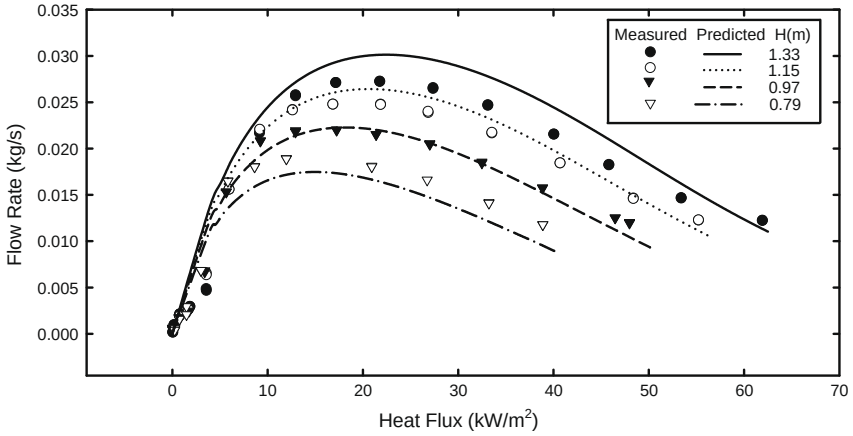

Fig. 4. Mass flow rate variation with increasing heat flux.

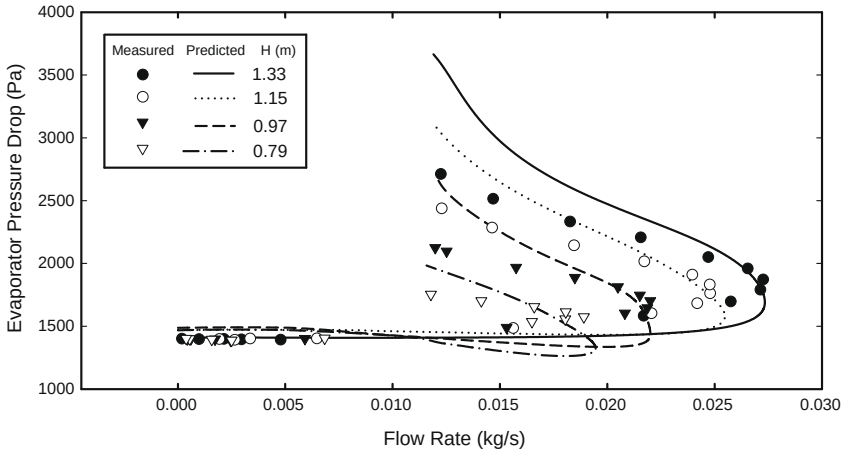

Fig. 5. Pressure drop variation across the microchannel evaporator plate with respect to mass flow rate.

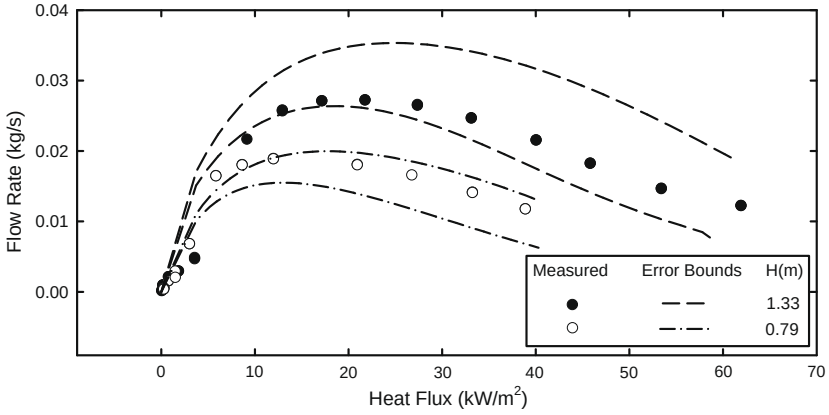

Fig. 6. Upper and lower bounds for predicted mass flow rates for $H = 1.33$ and 0.79 m.

Table 1
Experimentally observed limiting heat flux.

Condenser height, H (m)	Limiting heat flux, q_{lim} (kW/m^2)
1.33	61.91
1.15	55.20
0.97	47.98
0.79	38.89

cally different between the two condenser elevations. At each condenser elevation considered in this study, the flow regime within the riser is observed to be annular immediately prior to instability. Knowing that bubble coalescence and void fraction play a critical role in the fluctuation, it is quite reasonable that the fluctuations should not vary significantly between condenser elevations as observed in Figs. 7 and 8.

Once the heat flux is increased beyond the limiting heat flux, large scale fluctuations are observed in the flow field. Figs. 9 and

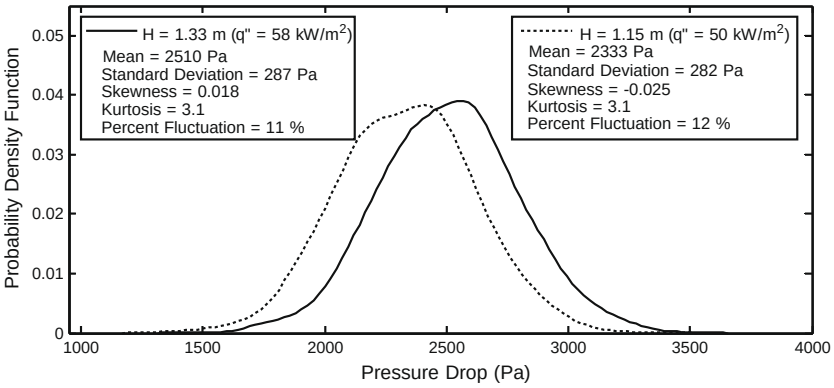

Fig. 7. Measured probability density function for pressure drop prior to unstable flow.

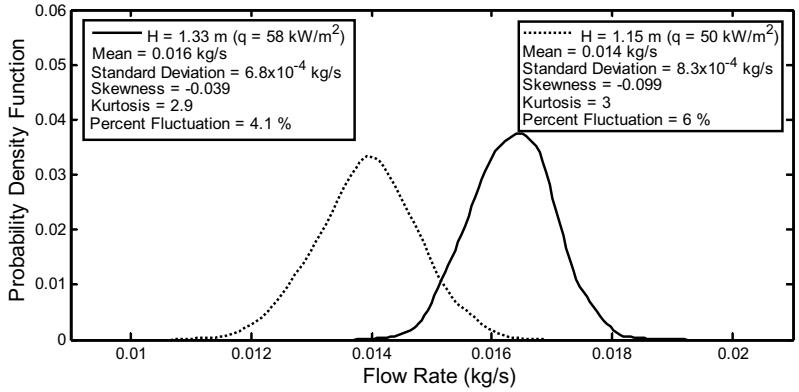

Fig. 8. Measured probability density function for mass flow rate prior to unstable flow.

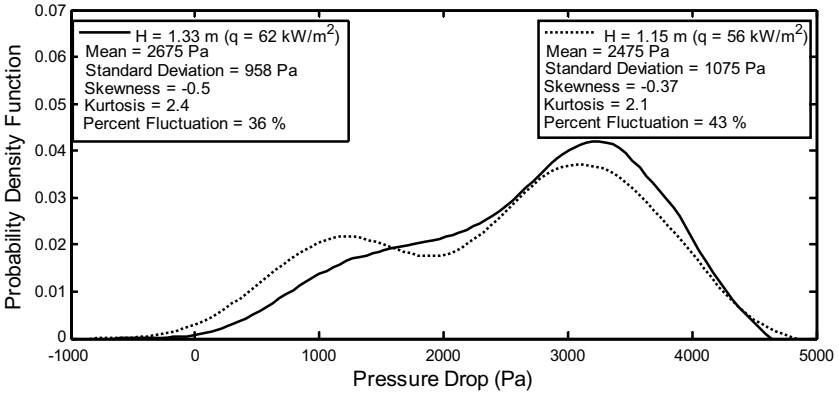

Fig. 9. Measured probability density function for pressure drop following the onset of unstable flow.

10 show the probability density functions for pressure drop and flow rate for $H = 1.33$ and 1.15 m slightly beyond the limiting heat flux. In each case the distributions resemble those for a sinusoidal signal in the time domain. There are two distinct peaks for both the pressure drop and flow rate. The flow rate is observed to go negative which is indicative of flow reversal. The average measured flow rate is 0.011 kg/s for each case. The flow rate has a positive skewness while the pressure drop has a negative skewness. This is most likely a result of the dependency of pressure drop on flow rate within the system. As the flow rate is increased the vapor quality decreases and vice versa. Since pressure drop is strongly dependent on vapor quality, the pressure drop is largest at low flow rates where vapor quality is largest. Therefore, it is expected that a positive skewness in the flow rate would result in a negative skewness in pressure drop as observed in Figs. 9 and 10.

A Fast Fourier Transform (FFT) was applied to the pressure drop and flow rate data taken at $H = 1.33$ and 1.15 m. Fig. 11 shows the power spectrum for mass flow rate, and the dominant frequency is approximately 0.8 and 1 Hz, respectively, for $H = 1.33$ and 1.15 m. The measured power spectrum indicates a very strong periodic low frequency fluctuation when the flow becomes unstable.

5. Instability prediction

In order to reliably predict the onset of instability, it is necessary to identify the controlling mechanism leading to the instability excursion. After giving consideration to the instability mechanisms described by Boure et al. [2] and Tadrist [15] it is concluded that the onset of the heat flux limiting instability observed in the thermosyphon facility is due to a static Ledinegg instability.

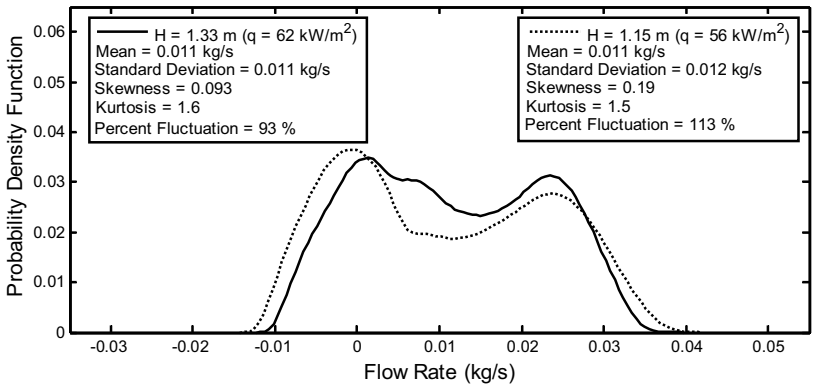

Fig. 10. Measured probability density function for mass flow rate following the onset of unstable flow.

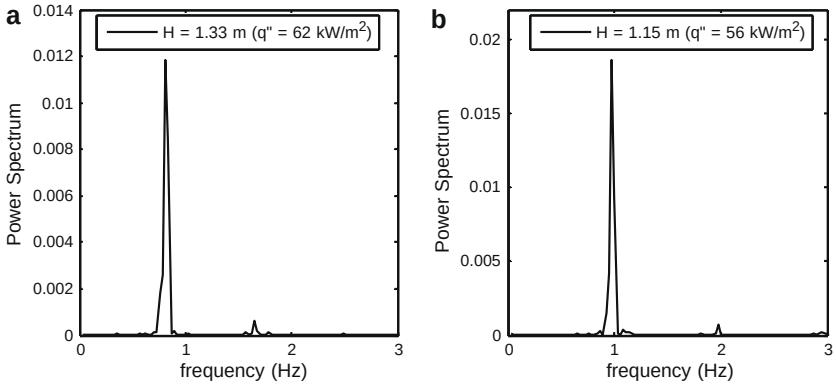

Fig. 11. Power spectrum for mass flow rate; (a) $H = 1.33$ m, (b) $H = 1.15$ m.

Such an instability involves a sudden change in the flow rate to a lower value followed by oscillations and ultimately system failure. In forced convection, the phenomenon is governed by the slope of pressure gradient with respect to mass flux for both the internal system characteristics (friction, acceleration, and gravity) and the external system characteristics (the pumping mechanism). In the case of natural circulation, the pumping mechanism itself is the gravitational pressure head exerted by the downcomer. The criterion for unconditionally stable flow is simply,

$$\frac{\partial \Delta P_s}{\partial G} > 0. \tag{18}$$

For the current facility, ΔP_s is the change in pressure between the condenser outlet and inlet and is zero for quasi-steady state operation. In order to investigate whether the system operation is stable, ΔP_s is first computed at each heat flux interval using Eq. (17). The quasi-steady state mass flux is that which gives zero pressure drop between the condenser inlet and exit and is determined for each heat flux interval. A perturbation in mass flux from the quasi-steady state, ΔG, of 5% is used based on the percent fluctuations revealed experimentally in Fig. 8. The change in system pressure drop resulting from a 5% perturbation in mass flux is approximated as follows,

$$\frac{\partial \Delta P_s}{\partial G} \approx \frac{\Delta P_s|_{G+\Delta G} - \Delta P_s|_G}{\Delta G}. \tag{19}$$

The system heat flux for which $\frac{\partial \Delta P_s}{\partial G}$ is negative is associated with unstable flow, and thus the limiting heat flux is that for which $\frac{\partial \Delta P_s}{\partial G} = 0$.

In order for the flow to transition to the unstable regime, the sum of the frictional, gravitational, and accelerational pressure change with respect to mass flux must be less than zero. Throughout the thermosyphon loop, the accelerational component of pressure drop is an order of magnitude smaller than the frictional and gravitational components and can be considered negligible here for discussion purposes. At high heat flux, where the instability occurs, the frictional pressure gradient within the microchannel plate is approximately 50 times the pressure gradient in the liquid downcomer section of the thermosyphon loop and 2.5 times greater than that in the two-phase riser section. Therefore the pressure drop across the microchannel plate, which is dominated by friction, gives a reasonable approximation of the shape of the frictional pressure drop with respect to mass flux throughout the system and is shown in Fig. 12 for illustration purposes.

In region-I, where the slope of the pressure drop as a function of flow rate curve is positive, a small perturbation decreasing the flow rate will result in increasing vapor quality and larger gravitational pumping potential. Simultaneously, the frictional pressure drop decreases due to decreased flow rate, and thus the flow rate will adjust back to its original value. Similarly, in region-I, the flow rate will return to its original value following a perturbation increasing the flow rate. Thus the flow is stable in region-I. In contrast, in region-II the slope of the pressure drop as a function of flow rate curve is negative, and a small perturbation increasing the flow rate will result in decreasing vapor quality and gravitational pumping potential. Simultaneously, the frictional pressure drop is reduced, and further increases in flow rate and decrease in vapor quality can result, until the flow swings back to region-I. However, the flow state does not remain in region-I for long due to the high heat flux and rapid increase in vapor quality. This behavior continues back and forth in an oscil-

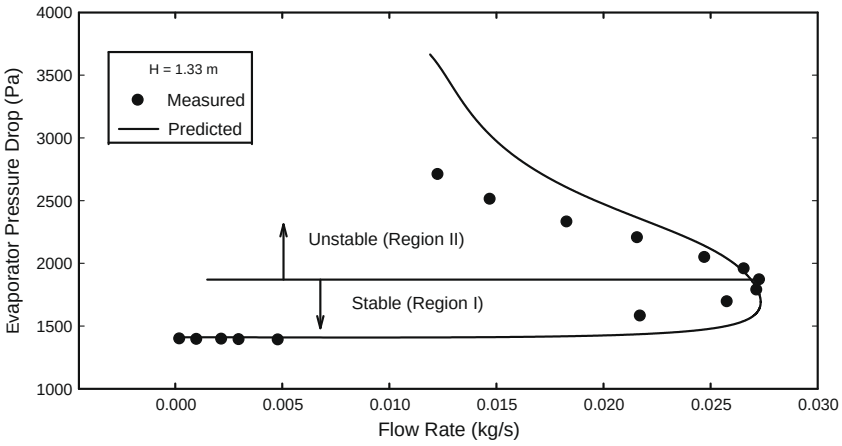

Fig. 12. Pressure drop across the microchannel plate for varying flow rate at $H = 1.33$ m.

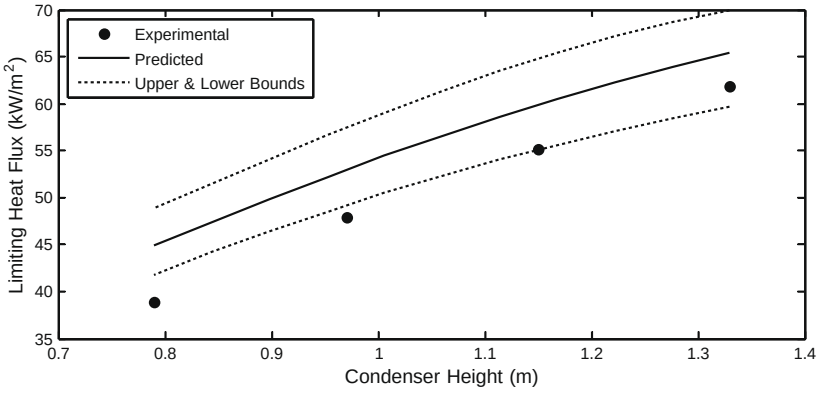

Fig. 13. Comparison of measured and predicted heat flux at the onset of instability.

latory mode until eventual dryout. It is noted that the flow in region-II may be stable as long Eq. (18) is satisfied.

Fig. 13 shows the computed limiting heat fluxes compared with those determined experimentally. Also shown are the upper and lower bounds of the computed limiting heat fluxes based on the uncertainties associated with the frictional pressure drop and vapor volume fraction predictions. The experimental measurements tend to fall on the lower bound of uncertainty. Given the complex nature of two-phase flow, the agreement is considered to be satisfactory.

6. Conclusion

The quasi-steady behavior of a two-phase microchannel thermosyphon has been investigated to obtain a quantitative understanding of the onset of unstable flow phenomenon observed at large heat fluxes. Static instabilities are largely influenced by the height of the condenser and stochastic variations in flow rate. A one-dimensional momentum equation-based model has been presented to provide a framework for predicting the onset of the instability. Reasonable agreement is obtained between the observed and predicted instability limiting heat flux.

Acknowledgment

Financial Support for this work was funded by NASA Glenn Research Center under contract NA63-2750.

References

[1] M. Ledinegg, Instability of flow during natural and forced circulation, Die Warme 61 (1938) 891–898.
[2] J.A. Boure, A.E. Bergles, L.S. Tong, Review of two-phase flow instability, Nucl. Eng. Des. 25 (1973) 165–192.
[3] M. Ishii, Study of flow instabilities in two-phase mixtures, ANL-76-23, 1970.
[4] A.E. Bergles, Review of Instabilities in Two-Phase Systems, Two-phase flows and Heat Transfer 1 (1977) 383–422.
[5] G. Yadiaroglu, Two-phase flow instabilities and propagation phenomena, in: J.M. Delhaye, M. Giot, M.L. Riethmuller (Eds.), Thermohydraulics of Two-phase Systems for Industrial Design and Nuclear Engineering, McGraw-Hill, New York, 1981 (chapter 17).
[6] K. Fukuda, T. Kobori, Classification of two-phase flow instability by density wave oscillation model, J. Nucl. Sci. Technol. 16 (1979) 95–108.
[7] S. Kakac, B. Bon, A review of two-phase flow dynamic instabilities in tube boiling systems, Int. J. Heat Mass Transfer 51 (2008) 399–433.
[8] I.S. Kyung, S.Y. Lee, Periodic flow excursion in an open two-phase natural circulation loop, Nucl. Eng. Des. 162 (1996) 233–244.
[9] M. Aritomi, J.H. Chiang, Geysering in parallel boiling channels, Nucl. Eng. Des. 141 (1993) 111.
[10] D.D.B. Van Bragt, Analytical Modeling of Boiling Water Reactor Dynamics, Delft University Press, 1998.
[11] X.T. Yang, S.Y. Jiang, Y.J. Zhang, Mechanism analysis on flow excursion of a natural circulation with low steam quality, Nucl. Eng. Des. 235 (2005) 2391–2406.
[12] G.V. Durga Prasad, M. Pandey, M.S. Kalra, Review of research on flow instabilities in natural circulation boiling systems, Prog. Nucl. Energy 49 (2007) 429–451.
[13] S.Y. Jiang, Y.J. Zhang, X.X. Wu, J.H. Bo, H.J. Jia, Flow excursion phenomenon and its mechanism in natural circulation, Nucl. Eng. Des. 202 (2000) 17–26.
[14] H.T. Lui, G. Kodak, S. Kakac, Dynamical analysis of pressure drop type oscillations with a planar model, Int. J. Multiphase Flow 21 (1995) 851–859.
[15] L. Tadrist, Review on two-phase flow instabilities in narrow spaces, Int. J. Heat Fluid Flow 8 (2006) 54–62.
[16] P. Garrity, J. Klausner, R. Mei, A flow boiling microchannel evaporator plate for fuel cell thermal management, Heat Transfer Eng. 28 (2007) 877–884.
[17] N. Zuber, J.A. Findlay, Average volumetric concentration in two-phase flow systems, J. Heat Transfer 87 (1965) 453–468.
[18] R. Muller-Steinhagen, K.H. Heck, A simple friction pressure drop correlation for two-phase flow in pipes, Chem. Eng. Process. 20 (1986) 297–308.
[19] P. Saha, N. Zuber, Point of net vapor generation and vapor void fraction in subcooled boiling, Proceedings of Fifth International Heat Transfer Conference 4 (1974) 175–179.